# Supporting Material: Representation of soil hydrology in permafrost regions may explain large part of inter-model spread in simulated Arctic and subarctic climate

**Philipp de Vrese[1,*], Goran Georgievski[1], Jesus Fidel Gonzalez Rouco[2], Dirk Notz[1,3], Tobias Stacke[1], Norman Julius Steinert[4], Stiig Wilkenskjeld[1], and Victor Brovkin[1,5]**

[1]Max Planck Institute for Meteorology, The Ocean in the Earth System, Hamburg, 20146, Germany
[2]University Complutense of Madrid, Department of Earth Physics and Astrophysics, Madrid, 28040, Spain
[3]University of Hamburg, Faculty of Mathematics, Informatics and Natural Sciences, Hamburg, 20146, Germany
[4]Norwegian Research Centre Climate and Environment, Bjerknes Centre for Climate Research, Bergen, 5007, Norway
[5]University of Hamburg, Center for Earth System Research and Sustainability, Hamburg, 20146, Germany
[*]philipp.de-vrese@mpimet.mpg.de

## S1 Comparison to observations (MPI-ESM)

| Var. | REF Bias (RMSE) | WET Bias (RMSE) | DRY Bias (RMSE) | W2D Bias (RMSE) | Source | Unit | Period | Fig. |
|---|---|---|---|---|---|---|---|---|
| $Temp_{2m}$ | 0.62 (3.16) | -0.85 (3.11) | 1.94 (3.67) | **0.04** (2.78) | GSWP3 | [K] | 1990 - 2014 | SF1 |
| MAGT | -1.95 (3.9) | -2.49 (3.8) | **-0.17** (2.77) | -1.70 (3.44) | GTNP | [K] | 2000 - 2010 | SF2 |
| $Thaw_{max}$ | 2.00 (2.30) | **0.08** (1.09) | 1.39 (1.85) | 0.27 (1.11) | CALM | [m] | 1990 - 2019 | SF3 |
| Precip | 8.42 (23.75) | 7.24 (23.61) | **4.59** (21.34) | 6.87 (22.97) | GSWP3 | [mm $mon^{-1}$] | 1990 - 2014 | SF4 |
| Snow | -16.46 (66.36) | **-12.67** (66.00) | -17.53 (66.78) | -15.18 (66.06) | CMC | [mm] | 1998 - 2012 | SF8 |
| Discharge | 295 | 275 | **234** | 279 | GRDC | [$km^3$ $yr^{-1}$] | 1980 - 1995 | SF9 |
| $cf_{Tree}$ | -4.3 (22.98) | -13.40 (24.38) | **-1.05** (25.95) | -12.22 (23.74) | ESACCI | [%] | 1992 - 2020 | SF6 |
| $cf_{Grass}$ | 24.48 (33.62) | 25.42 (34.72) | **20.23** (27.96) | 25.48 (33.60) | ESACCI | [%] | 1992 - 2020 | SF7 |
| $cf_{Shrub}$ | -5.58 (12.05) | -5.44 (10.14) | -7.01 (13.63) | **-4.71** (10.43) | ESACCI | [%] | 1992 - 2020 | SF8 |

**Supplementary Table ST1.** Overview over simulation biases in the northern permafrost regions for the different model setups, namely the reference model (REF), the WET setup, the DRY setup and the W2D setup. Given are the biases and root mean square errors for seasonally averaged 2m temperature relative to data from the Global Soil Wetness Project (GSWP3)[1,2], mean annual ground temperature (MAGT) relative to data from the Global Terrestrial Network for Permafrost (GTNP)[3–5], maximum annual thaw depths relative to data from Circumpolar Active Layer Monitoring (CALM)[6], mean seasonal precipitation relative to GSWP3 data, annual mean snow water equivalent relative to data from the Northern Hemisphere subset of the Canadian Meteorological Centre (CMC) operational global daily snow depth analysis[7], annual river discharge of the 5 largest Arctic rivers relative to data from the Global Runoff Data Centre (GRDC)[8] and tree-, grass- and shrub cover fractions relative to ESA Climate Change Initiative (ESACCI) data[9]. Bold numbers indicate the simulation exhibiting the smallest bias.

| Var. | REF Bias (RMSE) | WET Bias (RMSE) | DRY Bias (RMSE) | W2D Bias (RMSE) | Source | Unit | Period | Fig. |
|---|---|---|---|---|---|---|---|---|
| $Temp_{2m}$ | -0.60 (2.85) | -0.90 (2.93) | **-0.16** (2.68) | -0.65 (2.94) | GSWP3 | [K] | 1990 - 2014 | SF1 |
| Precip | **-1.39** (40.59) | -1.65 (40.18) | -1.49 (40.89) | -1.59 (39.54) | GSWP3 | [mm $mon^{-1}$] | 1990 - 2014 | SF4 |
| $cf_{Tree}$ | 4.73 (22.21) | **1.97** (22.71) | 5.23 (23.29) | 2.06 (22.36) | ESACCI | [%] | 1992 - 2020 | SF6 |
| $cf_{Grass}$ | 17.55 (27.1) | 17.56 (27.34) | **17.03** (25.60) | 17.97 (27.18) | ESACCI | [%] | 1992 - 2020 | SF7 |
| $cf_{Shrub}$ | -8.78 (15.28) | -8.74 (14.83) | -9.15 (15.74) | **-8.46** (14.90) | ESACCI | [%] | 1992 - 2020 | SF8 |

**Supplementary Table ST2.** Overview over simulation biases across all continental areas for the different model setups, namely the reference model (REF), the WET setup, the DRY setup and the W2D setup. Given are the biases and root mean square errors for seasonally averaged 2m temperature relative to data from the Global Soil Wetness Project (GSWP3)[1,2], mean seasonal precipitation relative to GSWP3 data and tree-, grass- and shrub cover fractions relative to ESA Climate Change Initiative (ESACCI) data[9]. Bold numbers indicate the simulation exhibiting the smallest bias.

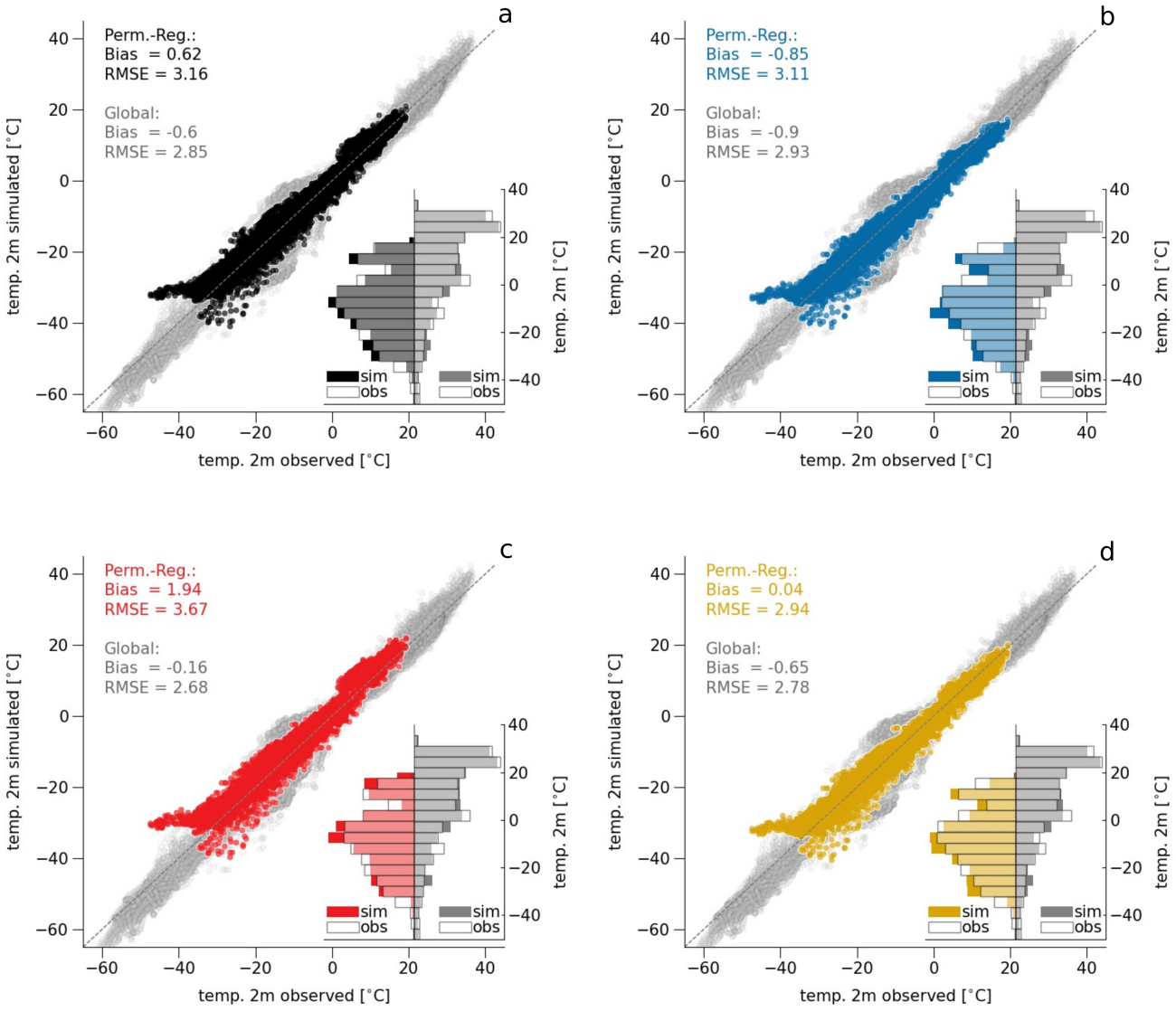


**Supplementary Figure SF1. 2m temperature**
Comparison of simulated and observation based (Global Soil Wetness Project (GSWP3)[1,2]) seasonally averaged 2m temperature for: a) MPI-ESM1.2 reference version (black), b) WET setup (blue), c) DRY setup (red) and d) W2D setup (yellow). The data is averaged over the period 1990 - 2014. In the main panel each dot represents one season and one grid-box, with the colored dots referring to the northern permafrost regions, while grey dots refer to all continental areas. The same color-coding is valid in the histogram on the bottom right.

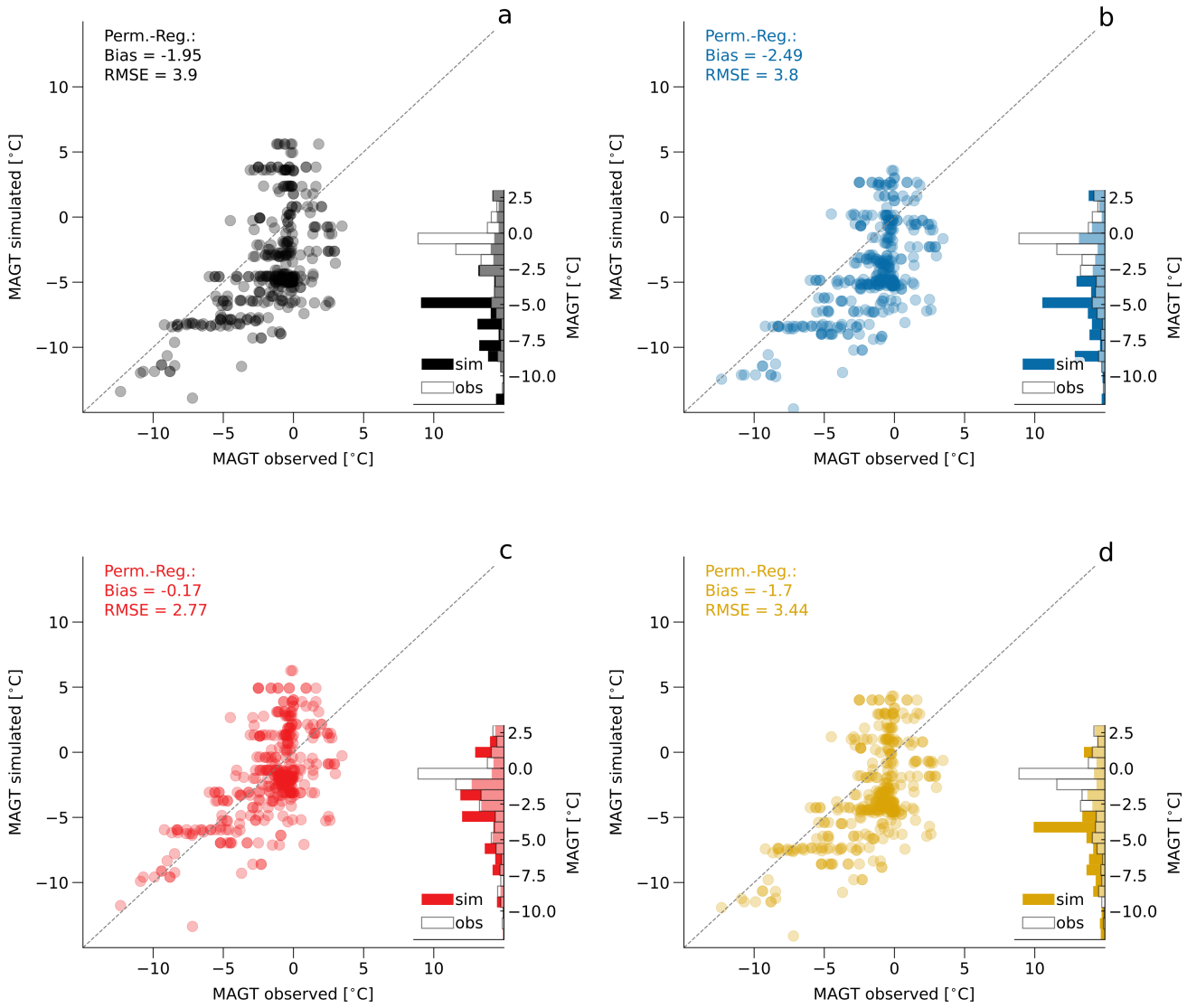


**Supplementary Figure SF2. Mean annual ground temperature**
Comparison of simulated and observed (Global Terrestrial Network for Permafrost (GTNP)[3–5]) mean annual ground temperatures (MAGT) in the northern permafrost regions for: a) MPI-ESM1.2 reference version (black), b) WET setup (blue), c) DRY setup (red) and d) W2D setup (yellow). For each site, the data is averaged over the period with available data between the years 2000 - 2010.

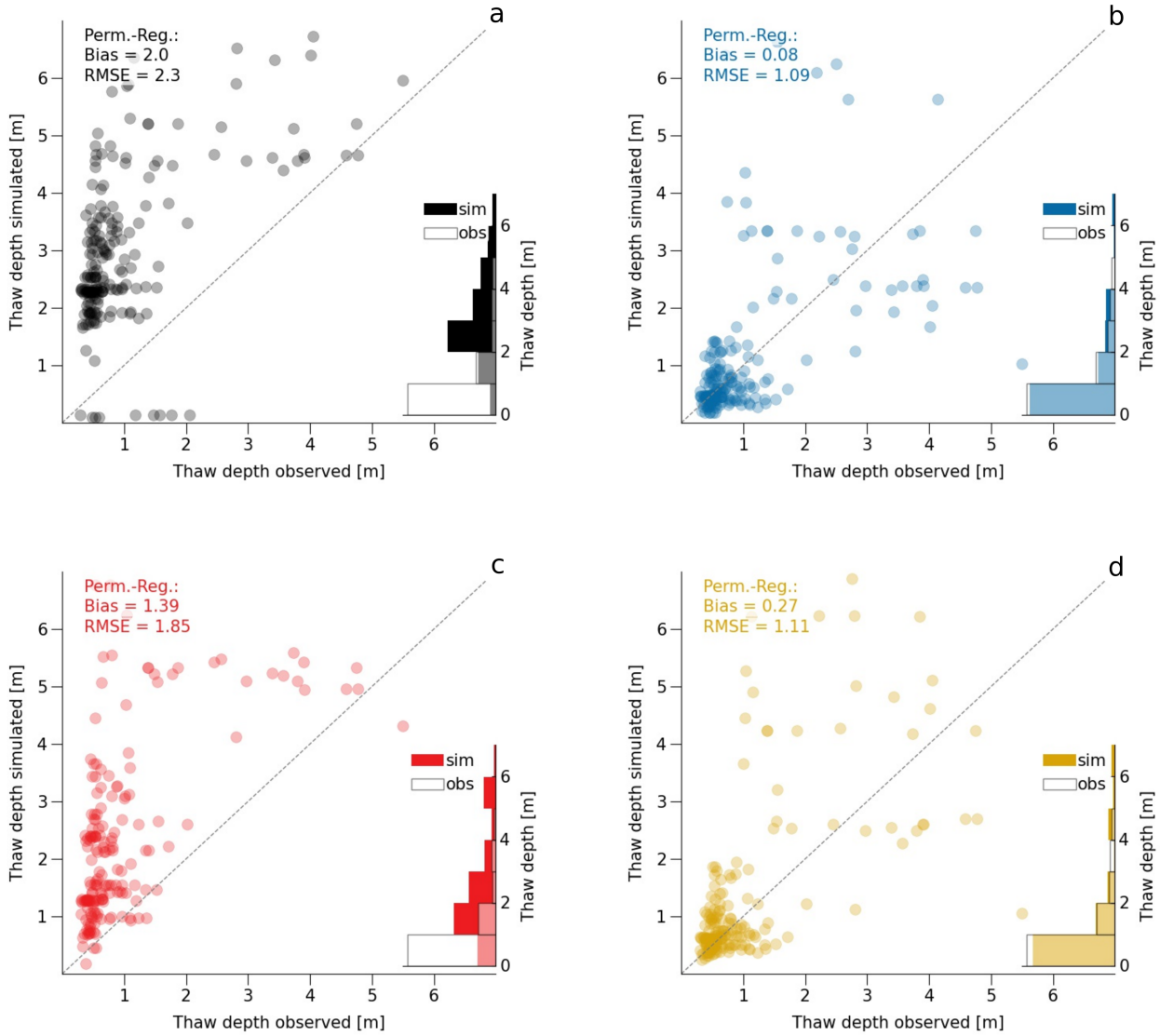


**Supplementary Figure SF3. Maximum annual thaw depth**

Comparison of simulated maximum annual thaw depths and observed end-of-season thaw depths (Circumpolar Active Layer Monitoring (CALM)[6]) in the northern permafrost regions for: a) MPI-ESM1.2 reference version (black), b) WET setup (blue), c) DRY setup (red) and d) W2D setup (yellow). For each site, the data is averaged over the period with available data between the years 1990 - 2019.

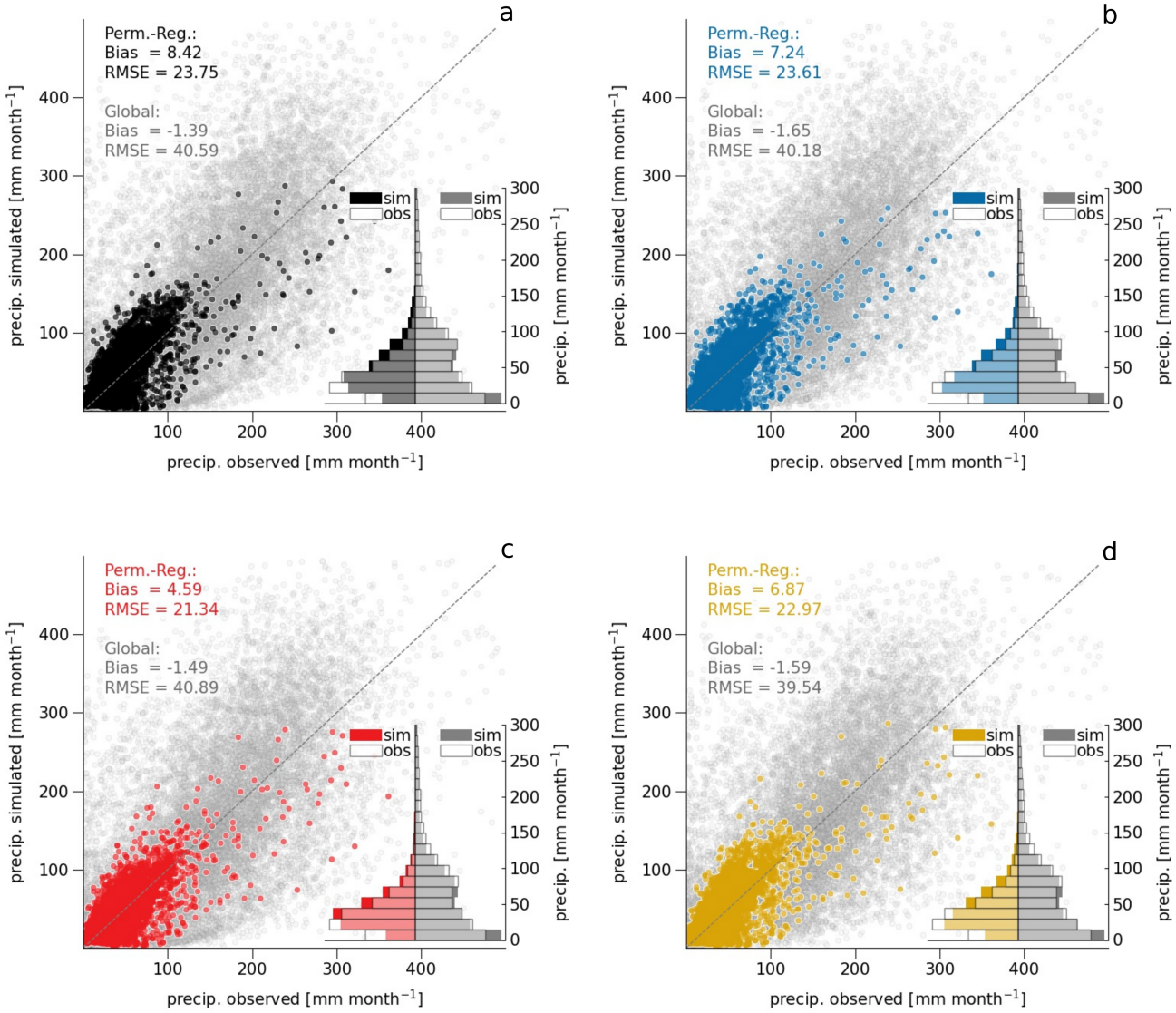


**Supplementary Figure SF4. Precipitation**
Comparison of simulated and observation based (Global Soil Wetness Project (GSWP3)[1,2]) seasonally averaged precipitation for: a) MPI-ESM1.2 reference version (black), b) WET setup (blue), c) DRY setup (red) and d) W2D setup (yellow). The data is averaged over the period 1990 - 2014.

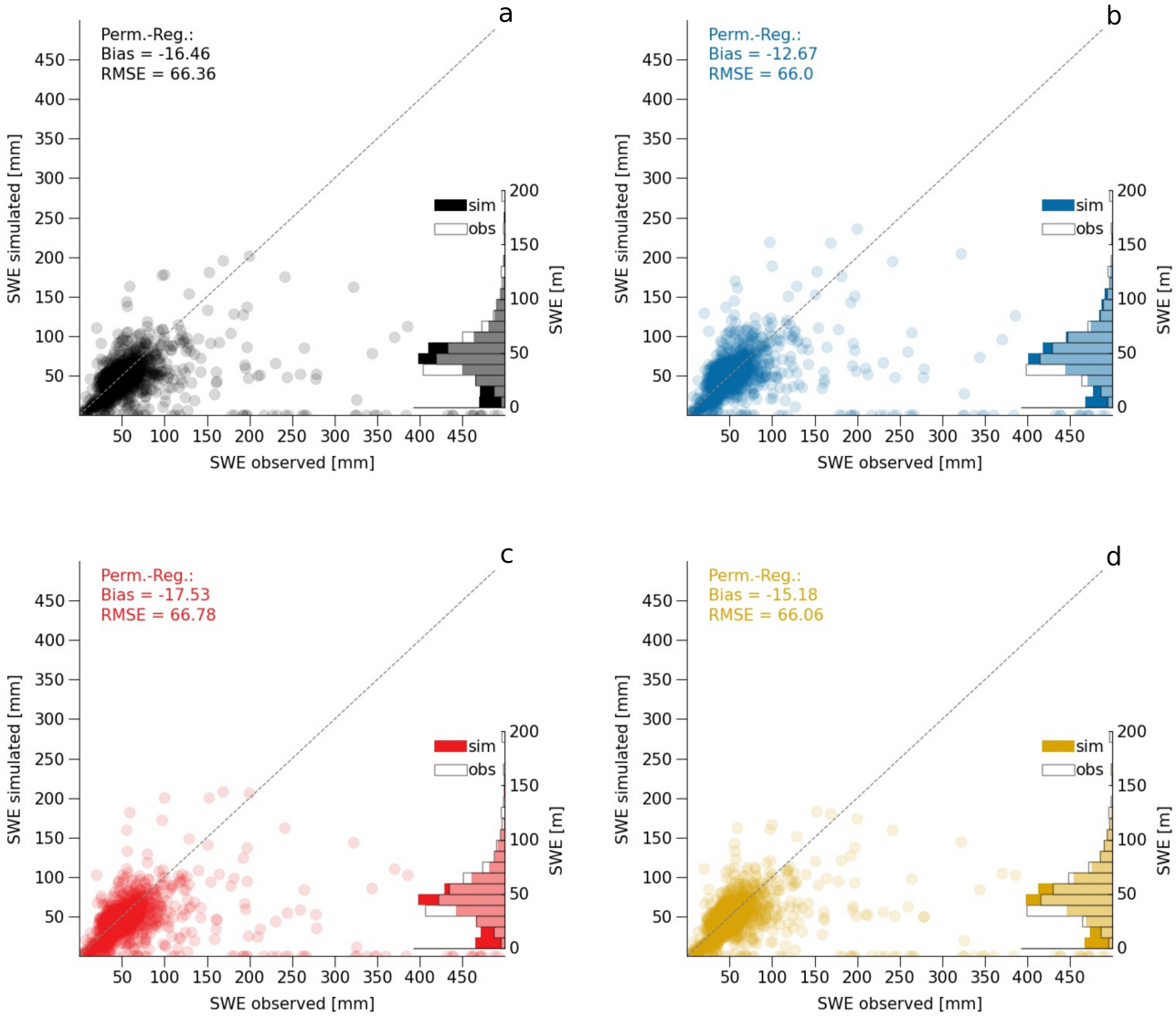


**Supplementary Figure SF5. Snow water equivalent**
Comparison of simulated and observed (Northern Hemisphere subset of the Canadian Meteorological Centre (CMC) operational global daily snow depth analysis[7]) annual average snow water equivalent in the northern permafrost regions for: a) MPI-ESM1.2 reference version (black), b) WET setup (blue), c) DRY setup (red) and d) W2D setup (yellow). The data is averaged over the period 1998 - 2012.

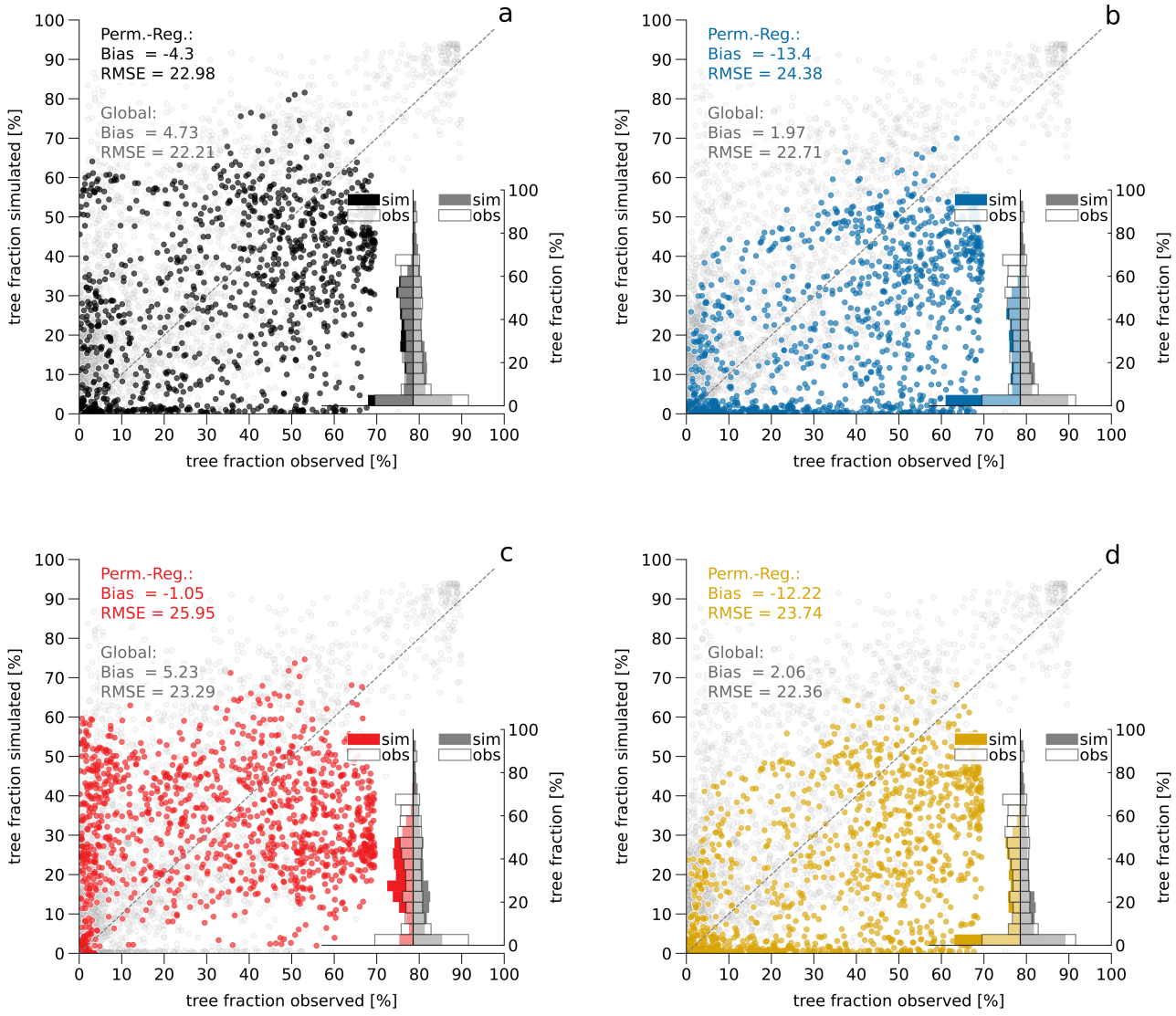


**Supplementary Figure SF6. Tree cover fraction**

Comparison of simulated and observed (ESA Climate Change Initiative (ESACCI)[9]) average tree cover for: a) MPI-ESM1.2 reference version (black), b) WET setup (blue), c) DRY setup (red) and d) W2D setup (yellow). The data is averaged over the period 1992 - 2020.

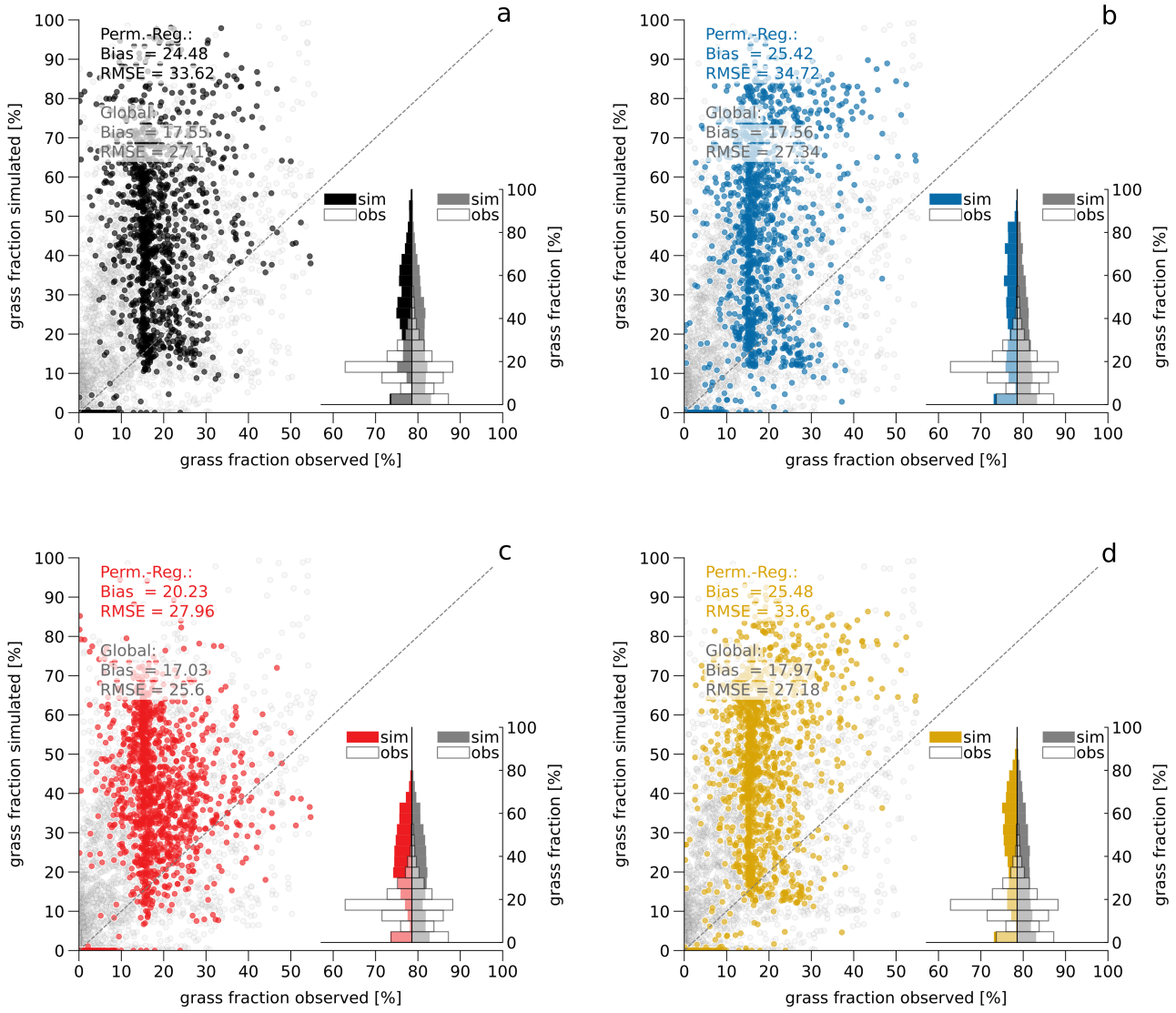


**Supplementary Figure SF7. Grass cover fraction**

Comparison of simulated and observed (ESA Climate Change Initiative (ESACCI)[9]) average grass cover for: a) MPI-ESM1.2 reference version (black), b) WET setup (blue), c) DRY setup (red) and d) W2D setup (yellow). The data is averaged over the period 1992 - 2020.

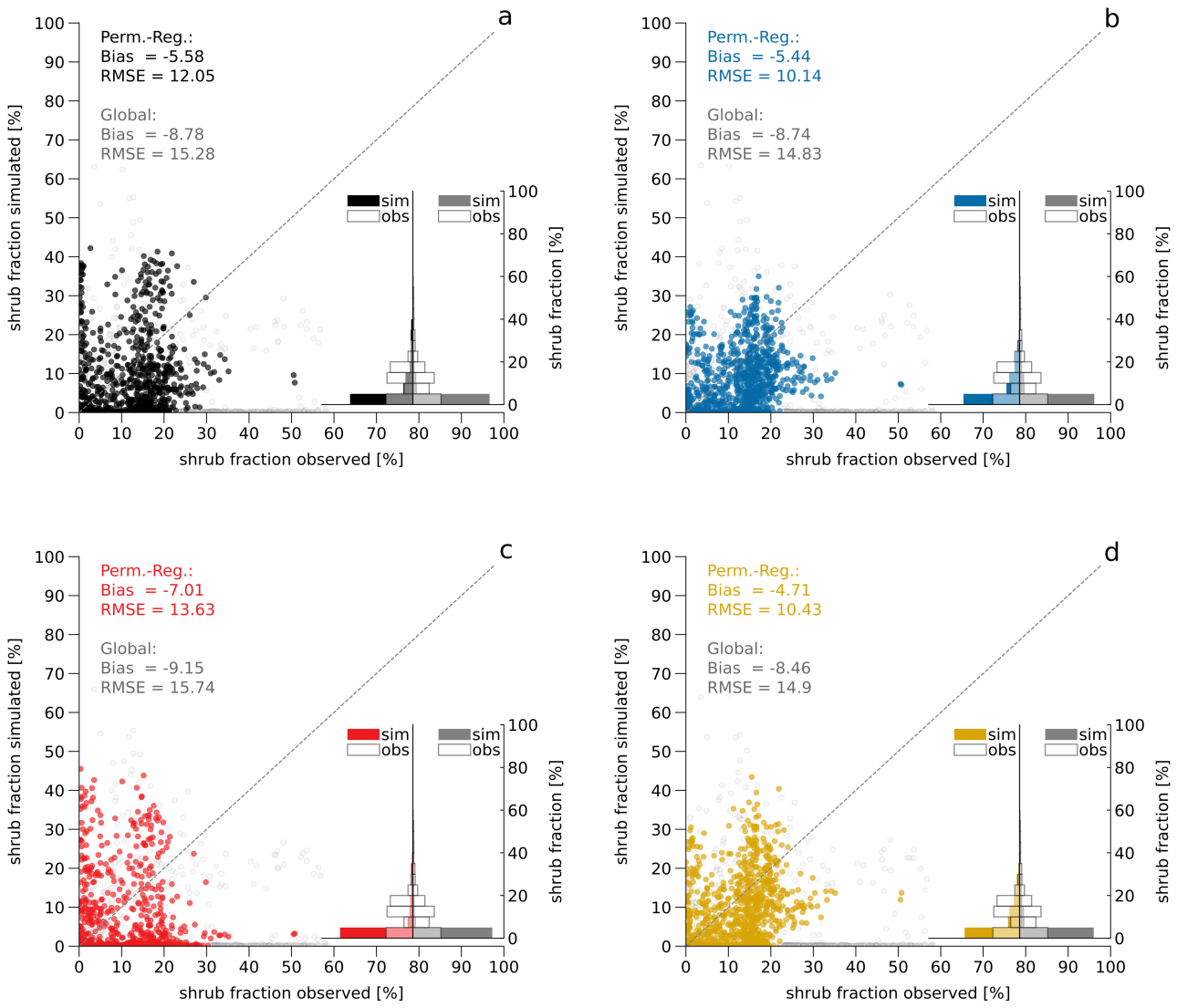


**Supplementary Figure SF8. Shrub cover fraction**
Comparison of simulated and observed (ESA Climate Change Initiative (ESACCI)[9]) average shrub cover for: a) MPI-ESM1.2 reference version (black), b) WET setup (blue), c) DRY setup (red) and d) W2D setup (yellow). The data is averaged over the period 1992 - 2020.

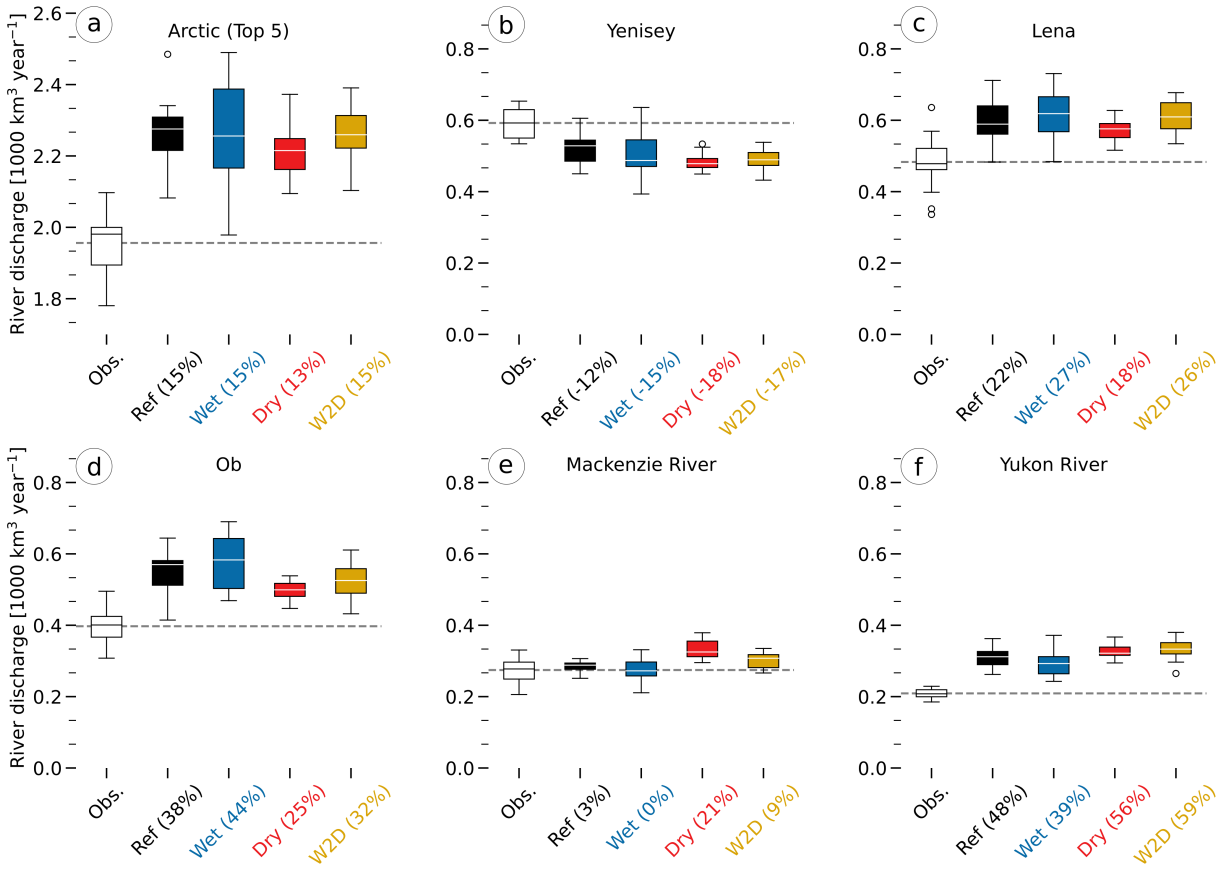


**Supplementary Figure SF9. Discharge**
Observed (white; Global Runoff Data Centre (GRDC)[8]) and simulated ( MPI-ESM1.2 reference version [black], WET setup [blue], DRY setup [red] and W2D setup [yellow]) annual river discharge of: a) the 5 largest Arctic rivers, b) Yenisey, c) Lena d) Ob, e) Mackenzie and f) Yukon. Values in brackets give the relative difference between the simulated and the observed discharge. For each river, the data is averaged over the period with available data between the years 1980 - 1995.

## S2 ICON-ESM

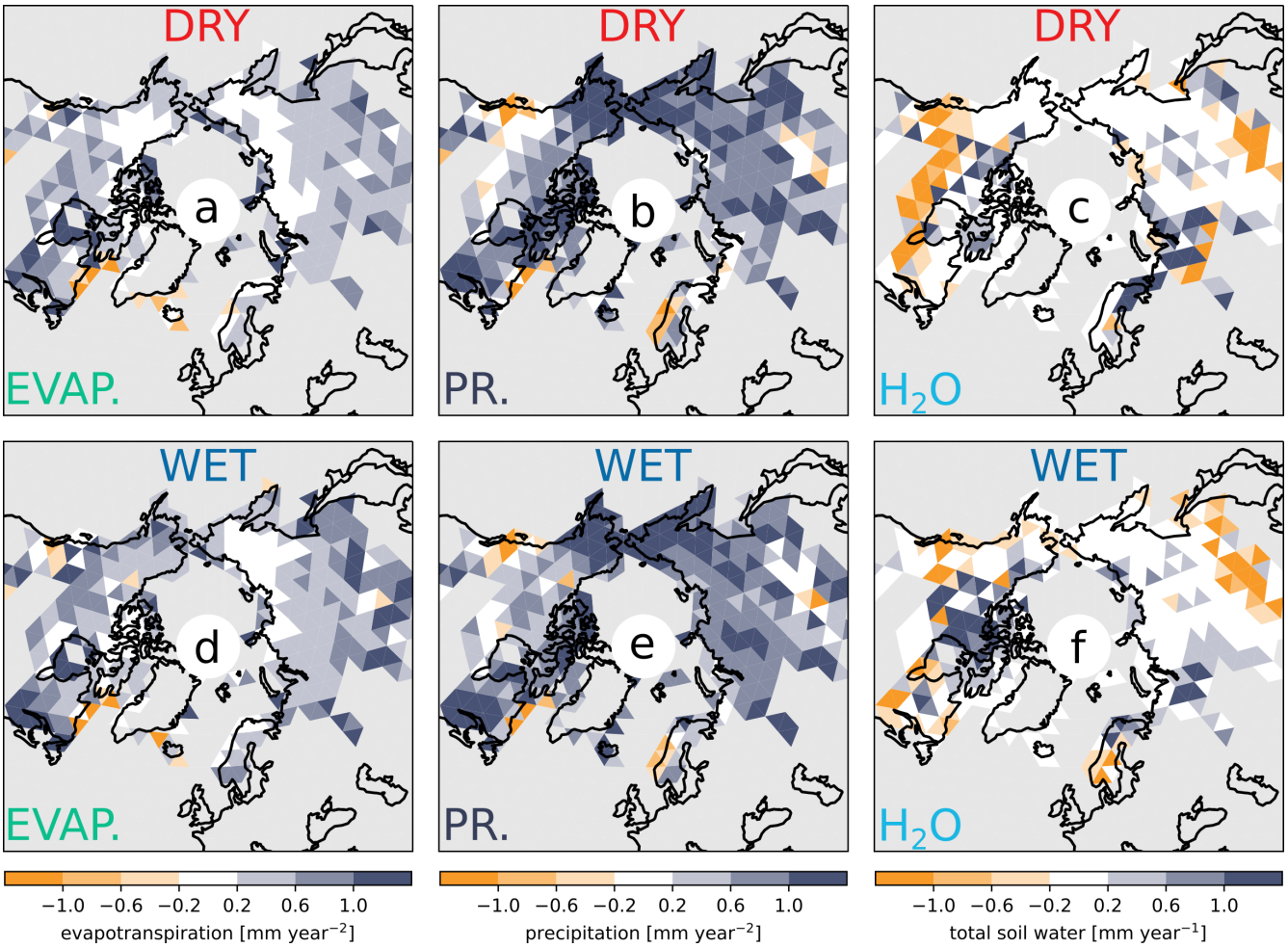


**Supplementary Figure SF10. Arctic futures in ICON-ESM**
a) 21st century precipitation trend simulated with the DRY ICON-L setup. b) Same as a) but for evapotranspiration. c) Same as a) but for the total soil water (liquid soil moisture and ice) content. d,e,f) Same as a,b,c) but for the WET ICON-L setup. Non-permafrost and glacier grid cells are shaded in grey.

Despite including neither the dynamic vegetation module nor the WEED module and despite being run at a lower resolution, the trends in precipitation and evapotranspiration compare well with the MPI-ESM simulations. However, in contrast to the latter, there are no clear general trends in the total soil water content, either in the DRY or in the WET ICON-L setups. While there are regions that exhibit notable in- and decreases in the total soil water in both simulations, these cancel out on the pan-Arctic scale.

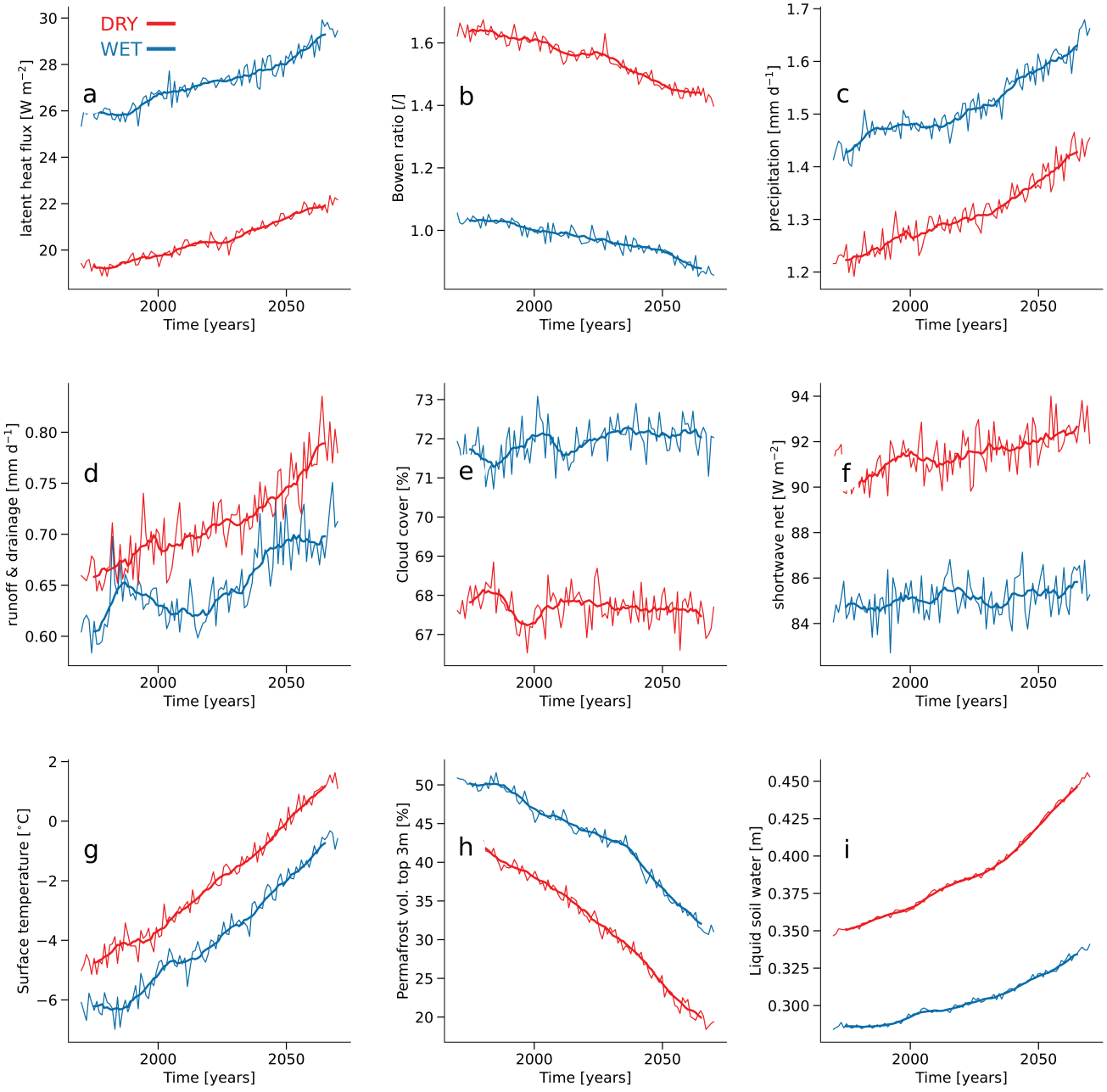


**Supplementary Figure SF11. Effects of soil hydrological conditions on near-surface climate:**
a) Latent heat flux in the northern permafrost regions in WET (blue) and DRY (red) ICON-ESM simulations for SSP5-8.5. Thin lines show the annual mean, averaged over the northern permafrost regions (note that that grid cells covered by glaciers were excluded), while thick lines give the 10-year running mean. b) Same as a) but showing the Bowen ratio, c) precipitation, d) surface runoff and drainage, e) accumulated cloud cover, f) solar radiation absorbed at the surface, g) surface temperatures, h) near-surface (top 3 m of the soil) permafrost volume and i) liquid soil water content.

The ICON-ESM produces a dryer climate than the MPI-ESM, with a lower cloud cover, less precipitation and, consequently, less evapotraspition, runoff and drainage. Due to the lower cloud cover, the surface shortwave net radiation is also higher, resulting in a higher sensible heat flux and consequently a much higher Bowen ratio. However, despite these differences in climate, the differences between the DRY and WET ICON-L setups generally agree well with those between the WET and DRY MPI-ESM runs.

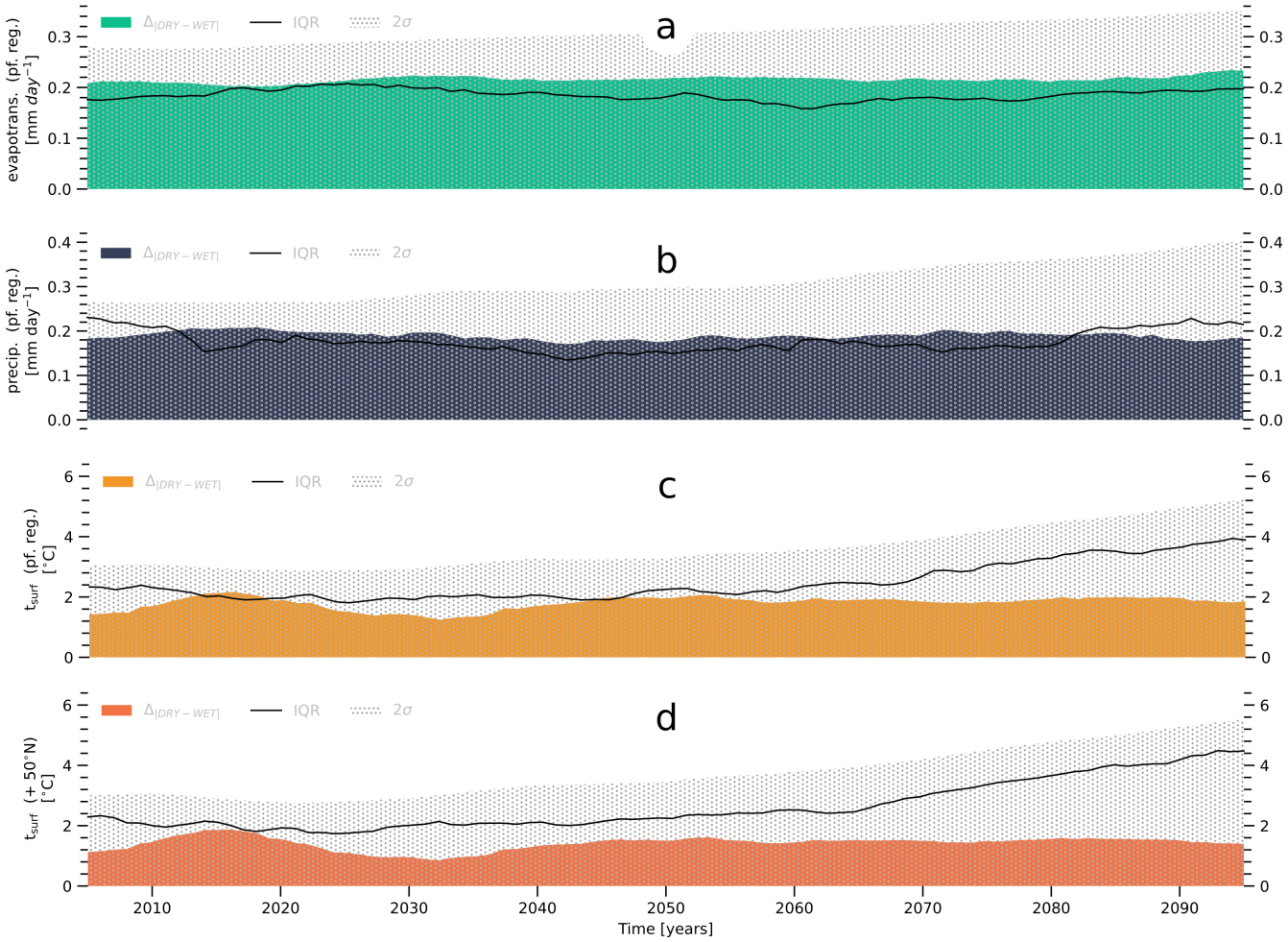


**Supplementary Figure SF12. Comparison to CMIP6 ensemble:**
a) Differences in evapotranspiration between the WET and the DRY ICON-L setup in permafrost regions ($\Delta^{evap}_{|DRY-WET|}$). Black line gives the interquartile range ($IQR^{evap}$) — that is the difference between the 75$^{th}$ and the 25$^{th}$ percentile — of the CMIP6 ensemble, while the dotted area provides 2 $\times$ the ensemble standard deviation ($2\sigma^{evap}$). b) same as a but for precipitation ($\Delta^{pr}_{|DRY-WET|}$, $IQR^{pr}$, $2\sigma^{pr}$), c) surface temperatures in permafrost grid cells ($\Delta^{ts}_{|DRY-WET|}$, $IQR^{ts}$, $2\sigma^{ts}$) and d) surface temperatures (land and ocean) north of 50°N ($\Delta^{ts;+50N}_{|DRY-WET|}$, $IQR^{ts;+50N}$, $2\sigma^{ts;+50N}$).

In general, the ICON-ESM simulations agree well with those using the MPI-ESM. However, the differences in the simulated temperatures between the DRY and the WET setups are substantially smaller in the northern permafrost regions (about 0.8°C, which corresponds to about 30 % of the temperature differences in the MPI-ESM simulations) and also those averaged across the latitudes 50°N to 90°N (about 0.6°C, also 30 % of the temperature differences in the MPI-ESM simulations).

## Supplementary References


1. Dirmeyer, P. A. *et al.* GSWP-2: Multimodel analysis and implications for our perception of the land surface. *Bull. Am. Meteorol. Soc.* **87**, 1381–1398 (2006).
2. Kim, H. Global soil wetness project phase 3 atmospheric boundary conditions (experiment 1) (2017).
3. Christiansen, H. H. *et al.* The thermal state of permafrost in the nordic area during the international polar year 2007-2009. *Permafrost and Periglacial Processes* **21**, 156–181 (2010). URL https://doi.org/10.1002/ppp.687.
4. Romanovsky, V. E., Smith, S. L. & Christiansen, H. H. Permafrost thermal state in the polar northern hemisphere during the international polar year 2007-2009: a synthesis. *Permafrost and Periglacial Processes* **21**, 106–116 (2010). URL https://doi.org/10.1002/ppp.689.
5. Smith, S. *et al.* Thermal state of permafrost in north america: a contribution to the international polar year. *Permafrost and Periglacial Processes* **21**, 117–135 (2010). URL https://doi.org/10.1002/ppp.690.
6. Brown, J., Hinkel, K. M. & Nelson, F. E. The circumpolar active layer monitoring (calm) program: Research designs and initial results1. *Polar Geography* **24**, 166–258 (2000). URL https://doi.org/10.1080/10889370009377698.
7. Brown, R. D. & Brasnett, B. Canadian meteorological centre (cmc) daily snow depth analysis data, version 1., cmc_swe_mly_clim_1998to2012_v01.2. NASA National Snow and Ice Data Center Distributed Active Archive Center, Boulder, Colorado USA (2010). URL https://nsidc.org/data/NSIDC-0447/versions/1. Accessed: 06.03.2021.
8. Grdc: Long-term statistics and annual characteristics of grdc timeseries data. Online provided by the Global Runoff Data Centre of WMO. Koblenz: Federal Institute of Hydrology (BfG) (2021). URL https://www.bafg.de/GRDC/EN/02_srvcs/21_tmsrs/210_prtl/prtl_node.html.
9. Georgievski, G. & Hagemann, S. Characterizing uncertainties in the ESA-CCI land cover map of the epoch 2010 and their impacts on MPI-ESM climate simulations. *Theor. Appl. Climatol.* **137**, 1587–1603 (2019).